Ab Initio Structure/Reactivity Investigations of Illudin-Based Antitumor Agents: A Model for Reaction *in vivo*

by **Laura N. Gregerson**, **Trevor C. McMorris**, **Jay S. Siegel**[1]), and **Kim K. Baldridge***[1])

Department of Chemistry, University of California-San Diego, La Jolla, CA 92093-0358, USA

This and the companion paper are dedicated to Professor *Duilio Arigoni* on the occasion of his 75th birthday. His work on the structures of natural products and the mechanisms and stereochemistry of biochemical processes strongly influences our course of study. *Non scholae sed vitae discumus.*

(Hydroxymethyl)acylfulvene (HMAF, irofulven; **4**), a third-generation derivative of a natural product extracted from the mushroom *Omphalotus illudens*, is selectively toxic towards certain forms of malignant tumors. Conversion of HMAF and cognates to stable aromatic derivatives is triggered by thiol attack *in vitro* and *in vivo*. Quantum-chemical methods predict well the structure for several functionalized derivatives of irofulven as compared to known X-ray crystallographic structures. Computational reaction profiles for thiol attack and aromatic rearrangement of irofulven and illudin S, a toxin from which irofulven is derived, provide insight into HMAF's selectivity and toxicity. Methods used include hybrid density-functional theory (HDFT), *Hartree–Fock* (HF), and *Møller–Plesset* second-order perturbation theory (MP2). Solvent effects have been explored by means of the new continuum-solvation method, COSab, presented in an accompanying paper.

Introduction. – Illudins are natural products isolated from the mushroom *Omphalotus illudens* [1–3]. Several analogues with slightly modified structures (**1**–**7**) that offer a range of therapeutic indices [4–6], a few of which have drawn considerable attention as potential drug candidates [5][7–13], have been synthesized. All derivatives bear common structural features and undergo a nucleophile-triggered addition/rearrangement cascade to a stable aromatic metabolite [6][14–17]. The details of this structural commonality and the mechanism of the addition/rearrangement process are key components in our understanding of the design of these therapeutic agents. In this work, we present accurate structure and property calculations on illudins **1**–**7**, with particular focus on illudin S = (2′*S*,3′*R*,6′*R*)-2′,3′-dihydro-3′,6′-dihydroxy-2′-(hydroxymethyl)-2′,4′,6′-trimethylspiro[cyclopropane-1,5′-[5*H*]inden]-7′(6′*H*)-one; **1**) and irofulven (= (6′*R*)-6′-hydroxy-3′-(hydroxymethyl)-2′,4′,6′-trimethylspiro[cyclopropane-1,5′-[5*H*]inden]-7′(6′*H*)-one; **4**). Specific reaction profile studies, performed for **1** and **4**, provide valuable insights into the energetics as well as the mechanism of action of illudins.

Functional-group analysis of the illudin family reveals three important substructures: an α,β-unsaturated carbonyl, a sterically congested spirocyclopropane ring, and a fulvenoid ring. The highly reactive and toxic parent compounds **1** and illudin M (= (3′*R*,6′*R*)-2′,3′-dihydro-3′,6′-dihydroxy-2′,2′,4′,6′-tetramethylspiro[cyclopropane-

[1]) Present address: Institute of Organic Chemistry, University of Zürich, Winterthurerstrasse 190, CH-8057 Zürich.

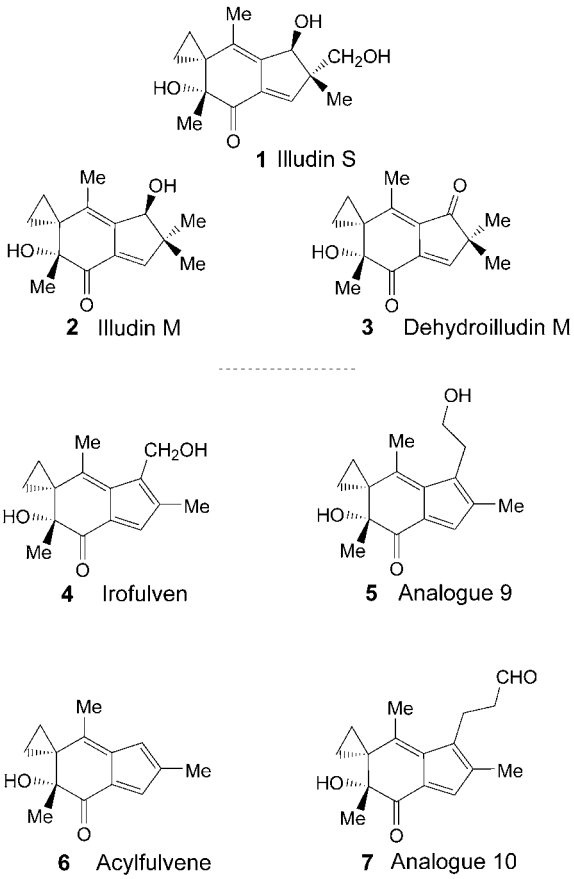

1,5′-[5*H*]inden]-7′(6′*H*)-one; **2**) contain the first two substructures, whereas the more-selective derivative **4** has, in addition, the third substructure.

The reactivity of the illudins has been studied *in vitro* [6][14–17]. At physiological pH, illudins do not react with common intracellular nitrogen-, oxygen- or halogen-based nucleophiles. In contrast, under similar conditions, illudins do react with sulfur nucleophiles, such as cysteine or glutathione, to produce an aromatic phenol derivative [15]. The first phase of the reaction is postulated to proceed by a *Michael* addition of the thiol anion to the α,β-unsaturated carbonyl (*Scheme 1*). Subsequently, nucleophilic attack opens the cyclopropane ring with concomitant loss of OH from the adjacent C-atom; if the second nucleophile is H_2O, the second reaction is equivalent to a rearrangement with aromatization. A potential link between illudin toxicity and reactivity toward thiols in the cell has been established by *McMorris et al.* [14][15], who explicitly demonstrated that illudins are more toxic to cells that have low levels of glutathione [15].

The parent illudins **1** and **2** show high cytotoxicity towards several tumor cell lines, but relatively low therapeutic indices and, therefore, are not optimal candidates for use

Scheme 1. *Mechanism Proposed for the Action of* **4** *at Physiological pH*

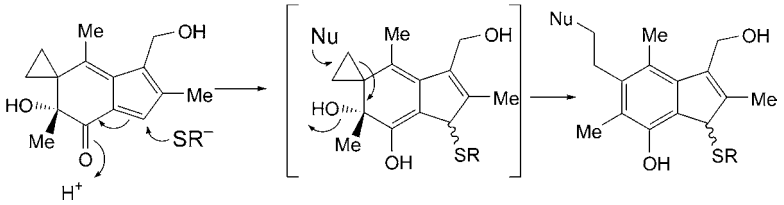

in vivo [1][9]. *McMorris et al.* have synthesized multiple derivatives of these illudins in attempts to find candidates that retain toxicity *but* exhibit increased selectivity towards tumor cells [4–7][14]. In particular, the third-generation derivative **4** is now in clinical trials. Thus, the comparison of **1** and **4** is key to understanding illudin-based therapies.

Computational Methods. – All calculations have been carried out with the GAMESS [18][19], and Gaussian98 [20] software packages. The computations employ a variety of levels of theory for comparative purposes. The wave-function-based methods considered include *Hartree–Fock* (HF) [21], second-order *Møller–Plesset* perturbation theory (MP2) [22][23], and several hybrid density-functional theory (HDFT) methods [24–26] based on *Kohn–Sham* orbitals [27] including the exchange-correlation functional combinations B3LYP [28–30], B3PW91 [28][31–34], and MPW1PW91 [35]. The optimal methodology to use was chosen after computations were performed on the lead target compound **4** with these wave-function methods in combination with a variety of basis sets, including 6-31G(nd,mp) ($n=1, 2$; $m=0, 1$) [36–39], DZ(2d,p) and DZV(2d,p) [40][41]. For each optimized geometry, the Hessian (matrix of second derivatives) was calculated to determine local minima (positive definite) or *n*th-order saddle point (*n* negative eigenvalues). Zero-point-energy corrections were calculated from the results of the Hessian computations. Visualization and analysis of structural (including representation of 3D molecular orbitals) and properties were performed with QMView [42], and MacMolPlt [43].

A level of chemically meaningful methodology to guide the experimental studies was determined by evaluating structure variance with increasing sophistication of basis set and addition of dynamic electron correlation. Such an investigation revealed the necessity for dynamic correlation and no less than double-ζ valence-plus polarization level, for which the results from B3LYP/DZV(2d,p) provide a high degree of reliability. In the case of the reaction phase studies, it was also necessary to include solvent effects, as specified below.

The gas- and solution-phase reactions of **4** and **1** with thiol were investigated by means of the intrinsic reaction coordinate (IRC) [44][45]. From the fully characterized transition-state structures, the IRC was followed down to the reactants by means of the *Gonzalez–Schlegel* second-order method [46][47]. The IRC is the path of steepest descent in mass-weighted coordinates and provides a convenient definition of the reaction path. Because the gradient at the saddle point is zero, the IRC is initiated by making a small displacement of 0.15 sqrt(amu)-bohr in the direction of the single imaginary normal mode, followed by hypersphere minimization about that point. These computations were performed at the HF and HDFT levels, with the DZV(2d,p) basis-

sets. Selected stationary points along the reaction paths were also examined with second-order MP2 perturbation theory to compare effects of correlation to that of HDFT. Effects of basis set superposition error (BSSE) [48] were investigated and found to be negligible.

Investigations of solvation effects were performed with our new implementations of the COSab solvation method [49–51], in GAMESS at the HF and HDFT levels of theory. These calculations were performed from the optimized gas-phase structures, with the DZV(2d,p) basis set and a dielectric permittivity of $\varepsilon = 78.4$ as the values for H_2O at room temperature. The parameters of the cavity construction are 1082 points for the basic grid, 92 segments on a complete sphere, and a solvent radius of 1.3 Å. Atomic radii were taken from *Bondi* [52] and from *Klamt*, where available [53].

Discussion. – Preliminary quantum-mechanical computations on **1**–**7** at a variety of levels of theory established a reliable level of theory for the prediction of structure and properties. Of **1**–**7**, the structures **1** and **4** have been solved crystallographically [6][7]. The calculated structures for **1** and **4** are in overall good agreement with the experimental X-ray structures (*Table 1*). Correlation between the calculated and experimental values for **1** (**4**) gives an RMS deviation for bond lengths, bond angles, and torsion angles of 1.2 (0.7) pm, 0.9 (0.7)°, and 2.5 (2.2)°, respectively. One bond length that is something of an outlier is C(6)–C(13) of **1**, which is calculated to be 0.03 Å longer than that described in the experimental X-ray structure. The experimental value is at odds with the standard for such conjugated olefin bond lengths [54], and, thus, it is possible that there is some error in the reported value or positional uncertainty contributing to the experimental result. In the case of **4**, there are three molecules in the asymmetric unit of the crystal structure [7]. The calculated geometry was compared to the average experimental value, and the agreement is excellent.

A fragment-structure analysis categorizes **1**–**7** further as fulvenes (**4**–**7**) or not (**1**–**3**) (*Fig. 1*). This structural difference is reflected, for example, in differences in the respective bond lengths (*Table 2*) across all analogues (C(12)–C(11), C(12)–C(5), C(13)–C(6), C(13)–C(12); see atom numbering in *Table 1*). Within the group **1**–**3**, dehydroilludin M (=(6′*R*)-6′-hydroxy-2′,2′,4′,6′-tetramethyl-spiro[cyclopropane-1,5′-[5*H*]indene]-3′,7′(2′*H*,6′*H*)-dione; **3**) bears a carbonyl at C(11) that creates a second α,β-unsaturated carbonyl functionality in the molecule. Among **4**–**7**, acylfulvene (=(6′*R*)-6′-hydroxy-2′,4′,6′-trimethylspiro[cyclopropane-1,5′ -[5*H*]inden]-7′(6′*H*)-one; **6**) is distinguished as the only one that does not bear a substituent at C(11). These functional-group differences betray themselves through subtle changes in the illudin structure. For example, in **3**, the bond lengths C(4)–C(5) and C(5)–C(11) are longer

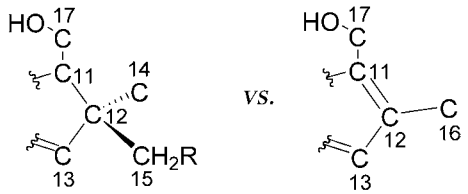

Fig. 1. *Fulvenoid character* (right) *of specific illudin analogues*

Table 1. *Bond Lengths* [Å] *and Angles* [°] (calculated[a]) and by X-ray crystal-structure analysis) *for* **1** *and* **4**

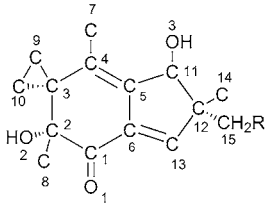

Illudin S (**1**)

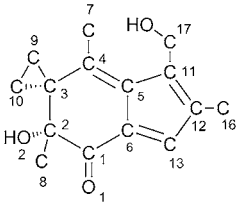

Irofulven (**4**)

	Calc.	X-Ray[b])	Calc.	X-Ray[c])			
				1	2	3	Avg.
C(1)–C(2)	1.531	1.522	1.534	1.527	1.534	1.527	1.529
C(2)–C(3)	1.546	1.543	1.543	1.537	1.544	1.547	1.543
C(3)–C(4)	1.504	1.495	1.492	1.496	1.492	1.498	1.495
C(4)–C(5)	1.351	1.336	1.371	1.365	1.357	1.361	1.361
C(5)–C(6)	1.462	1.459	1.464	1.467	1.467	1.463	1.466
C(6)–C(13)	1.349	1.317	1.369	1.359	1.368	1.360	1.362
C(13)–C(12)	1.512	1.508	1.458	1.449	1.451	1.451	1.450
C(12)–C(11)	1.574	1.570	1.383	1.381	1.370	1.368	1.373
C(11)–C(5)	1.522	1.518	1.467	1.470	1.475	1.475	1.473
C(1)–O(1)	1.223	1.213	1.229	1.239	1.227	1.229	1.232
C(2)–O(2)	1.413	1.418	1.413	1.428	1.416	1.415	1.420
C(2)–C(8)	1.544	1.527	1.546	1.531	1.535	1.539	1.535
C(3)–C(9)	1.516	1.515	1.520	1.525	1.518	1.507	1.517
C(3)–C(10)	1.526	1.518	1.520	1.525	1.527	1.536	1.529
C(4)–C(7)	1.505	1.501	1.503	1.502	1.508	1.500	1.503
C(1)–C(6)	1.469	1.476	1.445	1.436	1.450	1.448	1.445
C(9)–C(10)	1.510	1.491	1.503	1.494	1.494	1.493	1.494
C(3)–C(2)–O(2)	111.4	111.0	111.2	111.3	111.7	108.5	110.5
C(3)–C(2)–C(8)	110.4	110.3	110.1	109.9	109.9	109.6	109.8
C(2)–C(3)–C(9)	115.6	115.6	115.6	115.4	115.4	115.0	115.3
C(2)–C(3)–C(10)	117.2	118.4	117.2	118.6	117.8	117.1	117.8
C(12)–C(13)–C(6)	111.0	112.5	108.9	108.7	108.9	108.8	108.8
C(6)–C(1)–C(2)	114.1	114.8	114.5	114.9	114.3	115.0	114.7
C(13)–C(12)–C(11)	102.3	103.1	108.9	109.1	109.3	109.0	109.1
C(13)–C(6)–C(1)	127.9	128.5	129.8	130.3	129.5	128.5	129.4
O(1)–C(1)–C(6)	125.4	123.6	126.4	126.6	124.3	123.2	124.7
C(12)–C(11)–C(5)	104.7	104.8	107.7	107.7	107.6	108.0	107.8
O(2)–C(2)–C(3)–C(10)	– 25.1	– 23.4	– 23.3	– 16.2	– 24.8	– 22.0	– 21.0
C(9)–C(3)–C(2)–C(8)	– 78.9	– 75.4	– 77.2	– 69.7	– 75.6	– 76.9	– 74.1
O(2)–C(2)–C(3)–C(9)	42.2	43.5	43.4	50.4	41.8	44.2	45.5
C(11)–C(5)–C(6)–C(13)	7.9	– 2.8	– 2.2	– 1.9	– 3.5	0.4	– 1.7

[a]) B3LYP/DZ(2d,p). [b]) Data from [2]. [c]) Data from [5].

and shorter, respectively, than their counterparts in **1** and **2**, which lack the added conjugation; and, the sterically less demanding C(11) in **6** results in a shorter C(11)=C(12) double bond than that found for **4**, 'Analogue 9' (=(6′*R*)-6′-hydroxy-3′-(2-hydroxyethyl)-2′,4′,6′-trimethylspiro[cyclopropane-1,5′-[5*H*]inden]-7′(6′*H*)-one; **5**), and 'Analogue 10' (=(6′*R*)-6′-hydroxy-2′,4′,6′-trimethyl-7′-oxo-3′-(3-oxopropyl)spiro-

Table 2. *Calculated Bond Lengths* [Å] *and Angles* [°] *for* **1**–**7**[a])

	1	**2**	**3**	**4**	**5**	**6**	**7**
C(1)–C(2)	1.531	1.532	1.533	1.534	1.533	1.539	1.532
C(2)–C(3)	1.546	1.545	1.546	1.543	1.542	1.545	1.542
C(3)–C(4)	1.504	1.502	1.495	1.492	1.492	1.488	1.495
C(4)–C(5)	1.351	1.349	1.360	1.371	1.371	1.366	1.370
C(5)–C(6)	1.462	1.461	1.465	1.464	1.466	1.464	1.469
C(6)–C(1)	1.469	1.469	1.467	1.445	1.443	1.445	1.444
C(6)–C(13)	1.349	1.348	1.350	1.369	1.369	1.372	1.367
C(13)–C(12)	1.512	1.516	1.508	1.448	1.446	1.454	1.448
C(12)–C(11)	1.574	1.580	1.553	1.383	1.384	1.376	1.383
C(11)–C(5)	1.522	1.517	1.487	1.467	1.468	1.450	1.474
C(4)–C(7)	1.505	1.503	1.500	1.503	1.503	1.500	1.502
O(1)–C(1)	1.223	1.223	1.223	1.229	1.230	1.229	1.230
O(2)–C(2)	1.413	1.413	1.412	1.413	1.413	1.412	1.412
C(2)–C(8)	1.544	1.545	1.545	1.546	1.546	1.546	1.545
C(3)–C(9)	1.516	1.515	1.517	1.520	1.521	1.518	1.519
C(9)–C(10)	1.510	1.510	1.505	1.503	1.503	1.504	1.505
C(3)–C(10)	1.526	1.526	1.533	1.534	1.533	1.534	1.533
C(3)–C(2)–O(2)	111.4	111.1	111.0	111.2	111.1	110.9	111.1
C(3)–C(2)–C(8)	110.4	110.4	110.3	110.1	110.1	109.9	110.1
C(2)–C(3)–C(9)	115.6	115.9	116.0	115.6	115.5	116.3	115.4
C(2)–C(3)–C(10)	117.2	117.7	117.6	117.2	117.2	117.5	117.1
C(12)–C(13)–C(6)	111.0	111.6	111.3	108.9	109.0	108.9	109.0
C(6)–C(1)–C(2)	114.1	114.5	114.4	114.5	114.5	114.7	114.6
O(2)···C(10)	2.821	2.831	2.828	2.808	2.806	2.812	2.809
O(2)···C(9)	2.884	2.873	2.872	2.885	2.881	2.894	2.869
C(9)···C(8)	3.272	3.291	3.291	3.250	3.250	3.260	3.266
C(11)···C(13)	2.403	2.421	2.389	2.304	2.303	2.294	2.306
C(13)···O(3)	3.623	3.304	3.566	3.375	3.745	–	3.755
C(11)–C(5)–C(6)–C(13)	7.9	−8.2	−1.5	−2.2	−2.6	−1.1	−1.7
C(5)–C(4)–C(3)–C(2)	25.8	29.4	27.6	23.7	23.8	26.2	27.2
C(5)–C(6)–C(1)–C(2)	−24.5	−17.7	−19.7	−18.3	−17.9	−17.6	−17.2

[a]) See *Table 1* for atom numbering; calculations performed at the B3LYP/DZ(2d,p) level.

[cyclopropane-1,5′-[5*H*]inden-7′(6′*H*)-one] = 3-{(6′*R*)-6′-hydroxy-2′,4′,6′-trimethylspiro[cyclopropane-1,5′-[5*H*]inden]-3′(6′H)-yl}propanal; **7**).

In general, across all structural parameters, one finds the largest variations across the highlighted bonds in *Fig. 2*. Geometric features that are of particular importance to the postulated reaction process involve *a*) C(13) and neighboring functional groups, in light of the first step involving thiol attack, *b*) the functionality at C(11), which is known to greatly influence the reactivity of these compounds, and *c*) the conformation of the cyclopropyl ring relative to the groups attached to C(2). Overall, one would expect the isolated α,β-unsaturated carbonyl of **1**–**3**, to be more reactive than the acylfulvenoid unit in which the α,β-unsaturation is incorporated within a larger conjugated unit.

α,β-Unsaturated Carbonyl Component. The nucleophilic *Michael*-addition reaction of a thiol (*e.g.*, SH, H_2S, RSH, *etc.*) with an illudin occurs through attack at the β-C-atom (C(13)) of the α,β-unsaturated carbonyl. During such an attack, the hybridization of the orbitals of C(13) changes from sp^2 to sp^3. For **1** and **2**, this C-atom is already

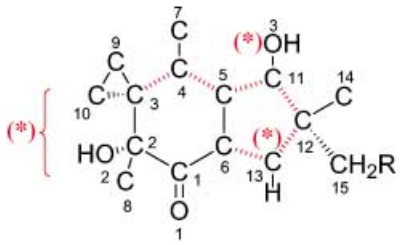

Fig. 2. *Sites of structural variance in* **1**–**7**

slightly hybridized before any such thiol attack, with an out-of-plane dihedral angle of close to 10° (*Table 3*). This distortion appears in the X-ray crystal data for **1** (H–C(13)–C(12)–C(11) = 7.5°), but not in the other analogues; thus, the five-membered ring is planar. The pyramidalization of the β-C-atom in **1** and **2** may favor nucleophilic attack at one face of C(13) by altering the orbital contribution to the LUMO.

Table 3. *Calculated Dihedral Angles* [°] *Involving C(13) for* **1**–**7**[a])

	1	**2**	**3**	**4**	**5**	**6**	**7**
H–C(13)–C(12)–C(11)	170.7	– 170.9	– 178.6	– 179.9	– 179.8	– 179.8	– 179.3
H–C(13)–C(6)–C(5)	178.8	180.0	179.8	– 179.0	– 178.9	– 179.8	– 179.9
H–C(13)–C(6)–C(1)	173.2	– 177.4	179.3	179.0	178.9	179.0	178.5

[a]) See *Table 1* for atom numbering; calculations performed at the B3LYP/DZ(2d,p) level.

Molecular-orbital analysis supports the electrophilic nature of these compounds at the β-C-atom of the α,β-unsaturated carbonyl. *Fig. 3* shows the lowest unoccupied molecular orbitals (LUMOs) for **1** and **4**. One can see that β-C-atom lobe for **4** is considerably larger than that of **1**, portending more-selective attack by a nucleophile.

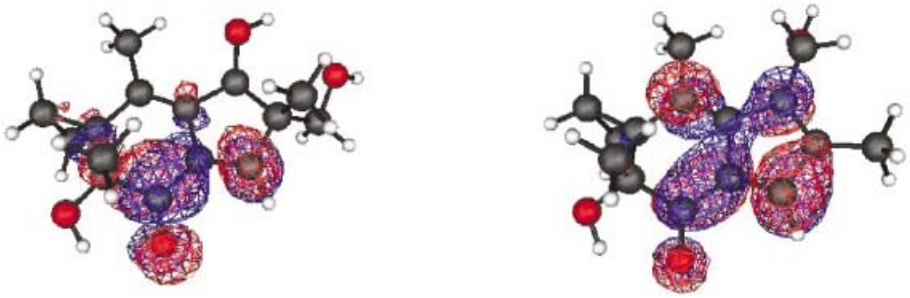

Fig. 3. *RHF/DZV(2d,p) LUMOs of* **1** *and* **4** (contour value is 0.03 Hartree)

Cyclopropyl Component. The proximity of the cyclopropyl ring (C(9) and C(10)) to the two substituents at C(2) (tertiary OH and CH_3(8) groups) correlates to the reactivity of **1** [6]. As noted in early crystal structure work [6], the six-membered ring is in an envelope configuration with C(2) above the plane, and the other ring C-atoms are approximately planar with those of the five-membered ring. The extent of the C(2) out-

of-plane angle in this envelope configuration also correlates with the extent of bond-alternation seen across C(3)–C(4) and C(4)–C(5). Analogues **1**, **2**, and **6** show significantly more bond alternation than the other four compounds, (~15 pm *vs.* 12 pm), which correlates with their greater out-of-plane deformation. The axial configuration of the Me on C(2) in this envelope configuration favors overlap of the Me–C(2) σ-orbital with the π^*-orbital of the carbonyl at C(1). Such an arrangement of orbitals facilitates the migration of the Me group from C(2) to C(1), which would lead to the formation of isoilludin [6].

The X-ray and calculated structures show a rather compressed moiety across the C(2)–C(3) region, with particularly short distances between the substituents at C(2) and C(3). The interatomic distances involved (*e.g.* O(2)···C(10), O(2)···C(9), and C(9)···C(8) in *Table 2*) are considerably shorter than what you would expect based on *Van der Waals* (VdW) approximations [52]. Across all analogues, the O–CH_2 distances are all less than 2.9 Å (VdW = 3.5 Å), and the Me–CH_2 distances all under 3.3 Å (VdW = 4 Å). This steric congestion suggests an increase in nonbonded repulsive interactions [6], and further rationalizes the tendency for the Me of C(2) to migrate to C(1), giving isoilludin S. Note also the correlation between the nonbonded C(8)···C(10) distances and C(10)···C(9) distances; the tighter the interaction across the C(2)–C(3) bond, the more stretched the cyclopropyl distance becomes, in an attempt to alleviate repulsive interactions.

Mechanistic Studies. – In experimental studies involving illudin analogues, their cell toxicity was attributed in part to electrophilicity [4][6][7][14]. Two highly toxic compounds, **1** and **2**, inhibit cell growth at an IC_{50} of 4 ± 1 nM (*Table 4*). The next-most-toxic analog in the set, which is **4** with an IC_{50} value of 73 ± 8, appears to be more selective for tumor cells.

Table 4. *Experimental* IC_{50}[a]) *Values Reported for* **1**–**7** [12]

Illudin analogue	IC_{50} [nm]
6	350 ± 20
3	310 ± 3
7	165 ± 55
4	73 ± 8
2	4 ± 1
1	4 ± 1
5	Insoluble

[a]) Tested in MV-522 cells.

Illudins react readily with sulfur nucleophiles at an optimal pH of *ca.* 6 [5][7][15]. The *Michael* addition of thiol to the α,β-unsaturated carbonyl group produces a cyclohexadienol intermediate that is rapidly converted to a stable aromatic structure by opening of the cyclopropane ring and loss of the OH at C(2) (*cf. Scheme 1*).

Reaction profiles provide an understanding of the mechanism and the nature of the energy barriers associated with the two phases of the reaction process, *a*) *Michael* addition to the α,β-unsaturated carbonyl, and *b*) cyclopropyl ring opening. Computations reveal a directing-group effect on the facial selectivity of thiol addition. For the

opening of the cyclopropane, there are several possible mechanistic proposals associated with the loss of OH, breaking of the C–C bond, and formation of the new nucleophile–C-atom bond. These include such possibilities as, *i*) nucleophilic attack on one of the methylene positions of the cyclopropyl, *ii*) internal nucleophilic attack from the adjacent OH group at C(2), and *iii*) explicit interaction of an external H_2O molecule either to stabilize the transition state from *ii*) or to act as the nucleophile, as in *i*), activated by interaction with the C(2)–OH.

Model-reaction profiles were constructed from stationary points obtained by optimized calculations at B3LYP/DZV(2d,p) level of theory as a model of the gas-phase reaction and followed by single-point computations by the COSab continuum solvent method at the higher basis [49–51]. The B3LYP/DZV(2d,p) level includes dynamic electron correlation and will be referred to here as HDFT, the RHF/DZV(2d,p) results referred to as HF (or set off in parentheses) are present for comparison but are inadequate for treating transition structures. The COSab method is described in detail in the accompanying paper. The energies derived from these single-point solvent computations are indicative of how the bulk dielectric of H_2O would perturb the gas-phase reaction, but these energies have not been derived in a manner to optimize the stationary points or include non-dielectric effects.

Michael-*Type Addition to the α,β-Unsaturated Carbonyl. Derivative Reaction Profile for* **4**. Thiol attack at the α,β-unsaturated carbonyl of **4** begins from a high-energy set of separated reactants in the gas phase that form a contact ion–molecule interaction stabilized by 19.8 (9.7) kcal/mol (*Fig. 4*). The gas-phase reaction shows almost no barrier to attack from the ion–molecule pair (0.1 kcal/mol by HDFT, 10.0 RHF) and two conformational isomers **A** and **B** are the predicted products. The transition state for thiol attack displays a C(6)–C(13)–S angle of 112.7° (114.1°) and a S–C distance of 2.56 Å (2.33 Å). The imaginary frequency was found to be 60.7 (290.9) cm^{-1} along a path associated almost exclusively with the out-of-plane motion of the β-C-atom combined with the approach of the S-atom. The energy difference between **A** and **B** by HDFT or HF methods favor **A** by about 3 kcal/mol, which is about the same as the energy difference between the ion–molecule complex and conformer **A**.

Conformers **A** and **B** are enolates, the C(1)–C(6) bond lengths are 1.38 Å and 1.39 Å, respectively. The key to the stabilization of conformer **A** over **B** is the potential to form a H-bond with the adjacent enolate O-atom when the thiol H-atom is rotated in that direction. The O(1)–H distance in form **A** of 2.21 Å (2.36Å) stabilizes it by 2.6 (3.1) kcal/mol over product **B** (*Fig. 5*). The transition state associated with the rotation of the thiol H-atom has an imaginary frequency of 141.1 (201.4) cm^{-1} and the calculated rotational barrier of 3.2 (3.8) kcal/mol (*cf. Fig. 4*). The reaction of thiol with **4** is exothermic overall by 22.8 (8.7) kcal/mol in the gas phase.

The significant difference in reaction profiles produced by HDFT and HF indicates the need for dynamic-correlation treatment, as is well known for weakly bound complexes and transition-state structures [55–57]. In particular, we note the dramatic increase in stabilization of the ion–molecule complex (by 10 kcal/mol) with the inclusion of dynamic correlation *via* HDFT methodology, and the subsequent decrease in barrier height from 10.0 kcal/mol to 0.1 kcal/mol; the ion–molecule complex is also significantly tighter with a S–C(13) distance of 2.9 Å *vs.* 3.8 Å.

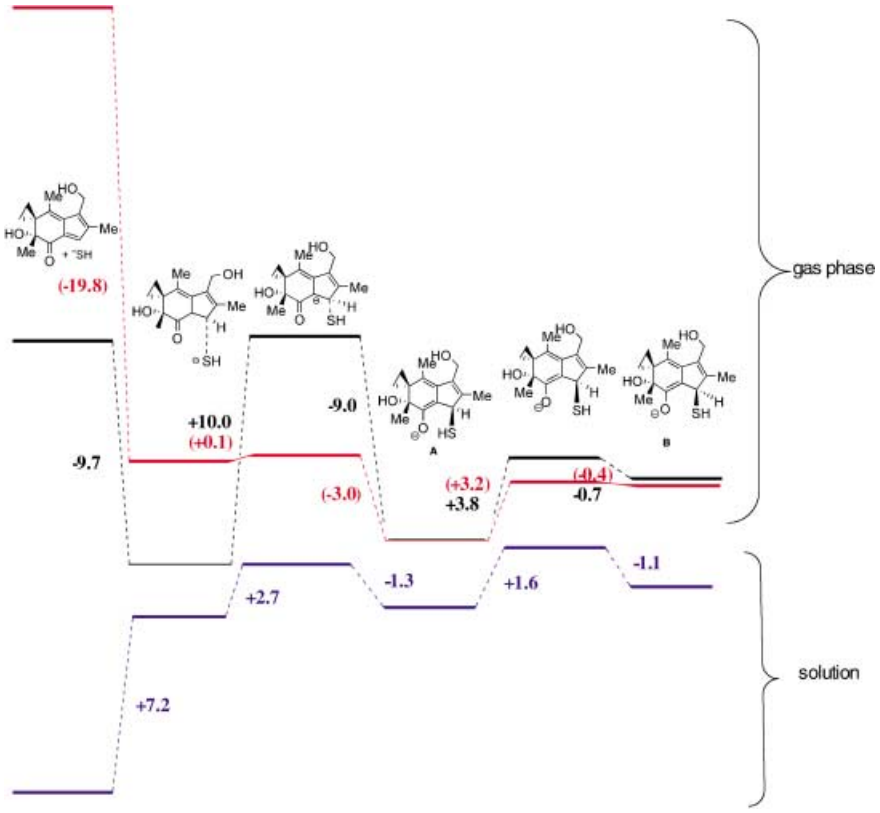

Fig. 4. *Reaction profile for the reaction of* **4** *with thiol, calculated at levels RHF/DZV(2d,p)* (black), *B3LYP/DZV(2d,p)* (red), *and B3LYP-COSab/DZV(2d,p)* (blue), *including the effects of zero-point energy*

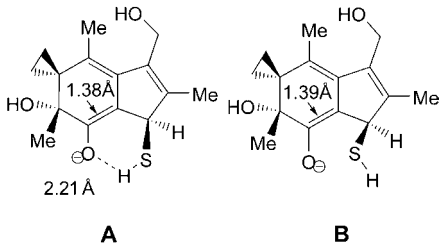

Fig. 5. *Comparison of bond lengths for conformers* **A** *and* **B**

Effects of a H_2O dielectric on the reaction process reveals that the ion–molecule complex is higher in energy than the separated reactants by 7.2 kcal/mol. The subsequent formation of the transition state from the initial ion–molecule complex is another 2.7 kcal/mol uphill; however, full optimization of the ion–molecule complex in a solution environment would likely show that the initial ion–molecule complex is not a stationary point but merely a shoulder on the energy surface between separated

reactants and the transition state (9.9 kcal/mol). The barrier between the transition state and conformer **A** (−1.3 kcal/mol) is similar for the solution and gas-phase study as is the ΔE between the two enolate conformers (+0.5 kcal/mol), **A** dominating over **B** with a smaller energy separation and barrier to interconversion. The overall reaction process in solution is endothermic by 8.6 kcal/mol, which suggests that thiol attack is rate determining for the more-selective agent **4**.

Derivative Reaction Profile for **1**. Investigation of the addition reaction of thiol with **1** reveals that the formation of the analogous ion–molecule from the separated reactants provides over twice the stabilization energy of that found for the reaction with **4** (34.3 and 37.4 *vs.* 19.8 kcal/mol). The thiol component remains the same in the two cases, therefore the additional energy must come from the inherent reactivity of **1**. In addition, reaction of thiol with **1** can proceed through two activated complexes, which differ in the face of attack at the β-C-atom, 'top'-TS3 *vs.* 'bottom'-TS4 (*Fig. 6*).

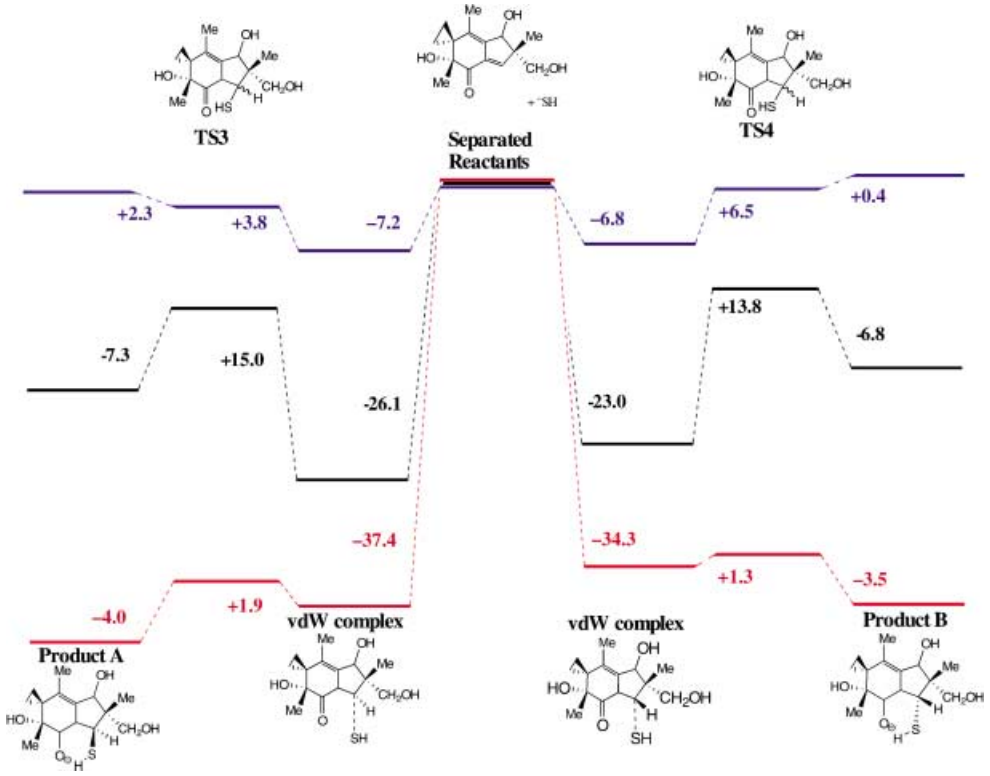

Fig. 6. *Reaction profile for thiol attack on* **1** via *TS3 and TS4, calculated at levels RHF/DZV(2d,p)* (black), *B3LYP/DZV(2d,p)* (red), *and B3LYP-COSab/DZV(2d,p)* (blue), *including zero-point-energy corrections*

On the basis of the C(13)–S distance of 3.16, 2.84, and 2.56 Å (2.40, 2.40, and 2.33 Å) for **1**(TS3), **1**(TS4), and **4**, respectively, SH^- attack on **1** occurs earlier in the reaction process than that observed for **4**. The reaction of **1** is also considerably more exothermic than that of **4**, which by the *Hammond* postulate predicts an earlier

transition state and less-selective kinetic reaction for **1** [58]. Additionally, attack on **4** disrupts the more-stable acylfulvenoid conjugation.

Initial SH^- attack on **1** is favored from the 'top' over 'bottom', $\Delta\Delta E$ 2.4 (2.4) kcal/mol, due to a favorable six-membered ring H-bonded complex between a stereochemically specific directing group and the incoming thiol (*Fig. 7,a* and *b*). Similar attack on **4** has no stereochemical preference and the primary OH group is one C-atom removed from the five-membered ring, which is suboptimal for directing this reaction (*Fig. 7,c*). Arms with optimized directing groups may well enhance the selectivity of action of these compounds (*Fig. 7,d*).

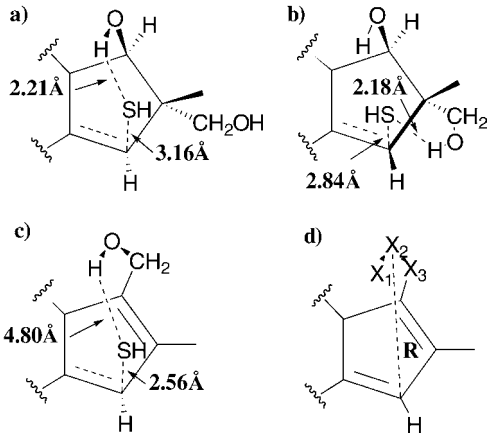

Fig. 7. *Transition-state structures* a) *TS3,* b) *TS4, and* c) *TS1, and* d) *definition of R*

Inclusion of the effects of a water environment on the reaction profile for thioxide attack on **1** makes the reaction nearly thermoneutral. Formation of the ion–molecule complex is accompanied by a larger kinetic cost compared to the gas-phase reaction, to reach the transition state and proceed to product formation. The overall reaction energetics are +1.0 and +0.0 kcal/mol for 'top' and 'bottom' attack, respectively. Similar top *vs.* bottom attack has also been observed experimentally [59].

Referring to the experimental IC_{50} values in *Table 4*, one can probe various structural components for their importance to antitumor activity. One might question the importance of the five-membered-ring component altogether. *Kinder et al.* [60]. synthesized bicyclic analogues of illudins **8** to investigate the relationship of the five-membered ring, and also, thereby, the β-C-atom needed for *Michael*-type addition, towards toxicity in the cell. The results of their investigation concluded with the observation that the fused cyclopentane ring was not required for antitumor activity. Additionally, the most-cyctotoxic analogues were those where R was rather small (*e.g.*, Me, vinyl). The role of the five-membered ring is more important for selectivity as expressed through the fulvenoid effect.

From the comparison of the reaction processes for **1** and **4** above, it would seem that the substituent at C(11) influences the activity of the resulting compound. There is the potential for the substituent at C(11) to act as an arm that stabilizes the attack of the incoming nucleophile, thereby facilitating nucleophilic reaction. Such an arm is present

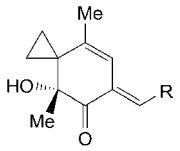

8

in **1**. This arm (*i.e.*, the CH_2OH substituent at C(11)), as represented in **4**, is still effective at assisting in the reaction (*cf. Fig. 7*); however, extension of the C(11) substituent arm by one C-atom (*e.g.*, CH_2CH_2CHO of **7**) appears to diminish reactivity, essentially eliminating the benefit of a ring transition state altogether. Likewise, the least-toxic analogue considered in this study, **6**, with no substituent at C(11), and no other functionality in the five-membered ring, has no possibility to form such a cyclic intermediate, diminishing reactivity by *ca.* 100-fold.

Cyclopropane Ring Opening. The second step of the illudin chemistry to consider is the opening of the cyclopropane ring to form the phenolic product (*cf. Scheme 1*). As previously noted [5], the product of thiol addition to **4** is highly reactive, readily attacked by an available nucleophile in solvent medium. In H_2O, one would expect protonation of the enolate O-atom to form an enol, from which there are several mechanistic possibilities to consider for cyclopropane ring opening: *i*) direct nucleophilic attack on the cyclopropane ring, *ii*) internal OH migration/cyclopropane ring opening, *iii*) nucleopilic attack assisted by the OH at C(2), and *iv*) stabilization of the transition state for internal OH migration by an explicit H_2O of solvation.

Intermolecular Nucleophillic Cyclopropane Ring Opening. Attack on the cyclopropane ring could occur directly from an external nucleophile, such as H_2O or OH^-, with subsequent loss of the external OH group (*Scheme 2*) [6]. Evidence that OH^- can be the attacking nucleophile comes from the isolation of ring-open products in which the thiol has been expelled.

Scheme 2. *Putative Mechanism for External Nucleophile Attack on the Cyclopropyl Group of* **4**

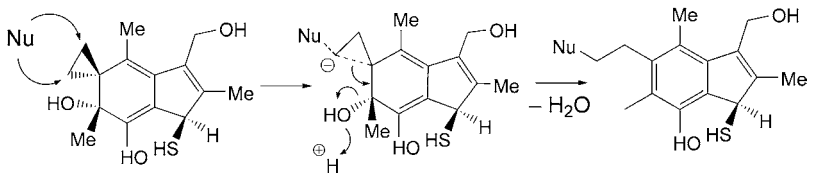

The RHF gas-phase-reaction profile for attack by OH^- is highly exothermic from separated reactants to separated products (*Fig. 8*). The energetics of ion–molecule complexes, intermediates and chemically meaningful transition species are strongly influenced by the lack of solvation of OH^- and all lie below the energy of the separated species. In fact, the solvation of OH^- is worth *ca.* 100 kcal/mol at this same level of theory according to our continuum solvation model. Although the RHF path shows a small barrier of 8.1 kcal/mol to a transition-state structure, which proceeds to products, when correlation is added *via* HDFT in the gas phase, ring opening appears to proceed through a process that involves expulsion of SH^-. No corresponding transition state was

located. Another consequence of this large solvation energy is that the side reaction involving the expulsion of SH^- is preferred in the gas-phase model. Our supposition is that this reaction proceeds instead by either a H_2O nucleophile attacking the cyclopropyl group or internal OH attack (shown below) facilitated by other nucleophiles that are also present, such as H_2O.

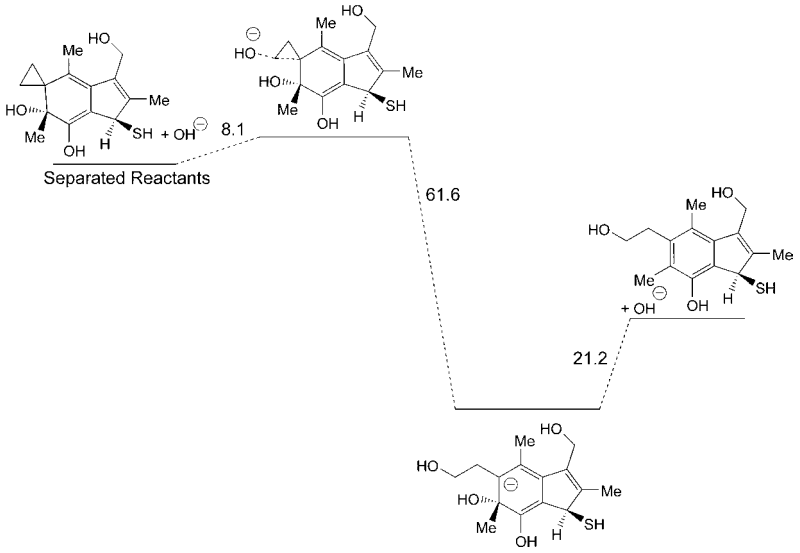

Fig. 8. *RHF Reaction profile for OH^- attack on the cyclopropane ring of* **4**

Hydroxy Migration/Cyclopropane Ring Opening. Internal attack by the tertiary OH group on the *syn*-methylene C-atom of the cyclopropane ring would form a four-centered transition state from which the open aromatic product could form directly (*Fig. 9*). The barrier to ring opening in this mechanism is 52.4 kcal/mol, and is an overall exothermic process in the gas phase, −33.1 kcal/mol. The energetics of the reaction differ by 3.2 kcal/mol in the aqueous environment. The activation energy drops to 49.3 kcal/mol and the reaction is predicted to be exothermic by 36.3 kcal/mol. Although the energy barrier is substantial in this model, catalysis of this reactive process within an enzyme, or with specific assistance from H_2O, is perhaps still feasible (see below).

In reactions involving **3**, a derivative related to an intermediate one might find along an internal OH reaction path has been isolated [5]. The structure of this tetrahydrofurano by-product **9** has been determined by X-ray crystallography [5].

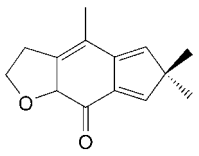

9

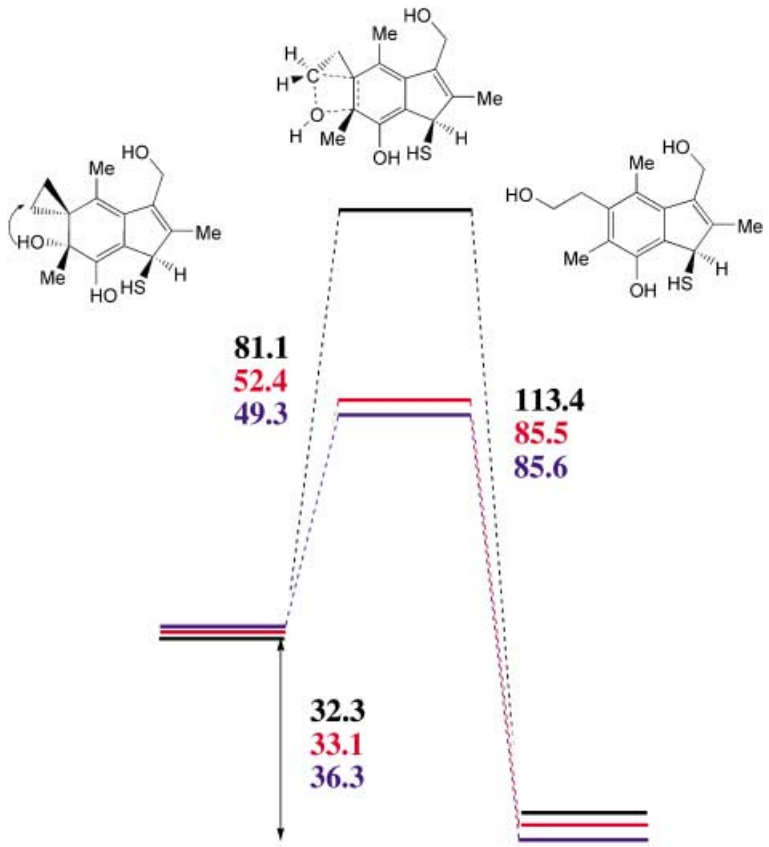

Fig. 9. *Reaction profile for intramolecular OH attack/migration calculated at levels RHF/DZV(2d,p)* (black), *B3LYP/DZV(2d,p)* (red), *and B3LYP-COSab/DZV(2d,p)* (blue)

The Role of an Explicit H_2O Molecule. Two scenarios for an explicit external H_2O molecule can be distinguished by whether the additional H_2O inserts itself between the OH^- group at C(2) and the cyclopropane ring or between the attacking internal OH group at C(2) and the enol OH group at C(1). Such processes could happen in H_2O but can not be described by any continuum solvent model.

In the first scenario, the cyclopropyl ring opens through an attack by an external H_2O molecule that acts as nucleophile and *Brønsted* acid simultaneously (*Fig. 10*, TSA). An alternative way of looking at this would be to consider the OH group at C(2) as an activator of the nucleophilicity of the incoming H_2O.

In the second scenario, a single H_2O molecule can form a seven-membered transition state (*Fig. 10*, TSB) and enable the opening of the cyclopropane ring with concomitant loss of the tertiary OH group (*Scheme 3*). The external H_2O acts as a *Brønsted* acid to activate the loss of OH^-. This activation is assisted by H-bond donation from the enol OH group, which, in turn, accepts a H-bond from SH. Such a cascade of incipient proton transfers is analogous to an intramolecular version of the

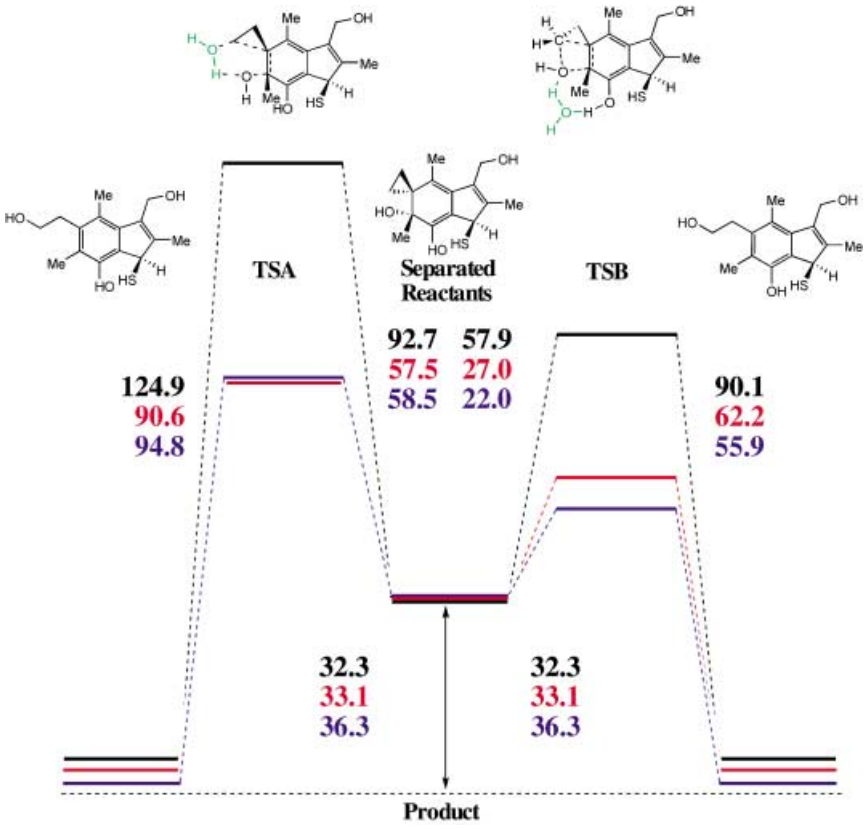

Fig. 10. *Reaction profiles for the explicit interaction of H_2O in the rearrangement of* **4**, *calculated at levels RHF/DZV(2d,p)* (black), *B3LYP/DZV(2d,p)* (red), *and B3LYP-COSab/DZV(2d,p)* (blue). H_2O acting as the attacking nucleophile assisted by the OH group at C(2) (TSA); H_2O acting to stabilize the internal attack of the OH group at C(2) (TSB)

Scheme 3. *Formation of Complex between H_2O, Secondary OH Group, and Cyclopropyl Group*

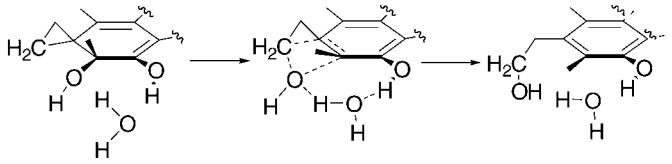

Grotthuss chain mechanism [61]. If this reaction proceeds more quickly along the OH^-/H_2O elimination coordinate than the nucleophilic attack coordinate, then the transition state may be considered more the interaction between the eliminated H_2O and an insipient cyclopropylcarbinyl ion [62]. The arylcyclopropylcarbinols are known to open stereoselectively to form butenols [63]. Solvolysis occurs in such systems between 10^6 and 10^9 times faster than with a simple alcohol [62]. If one adds to this the benefit of aromatization, considerable driving force is present for the reaction.

HDFT Results predict the activation energy for formation of TSA to be 57.5 kcal/mol, close to that of the internal OH^- attack mechanism; the overall reaction process is exothermic at −33.1 kcal/mol (*Fig. 10*). As expected, the effect of correlation is pronounced in this case due to the makeup of the transition state; RHF results place the barrier for such a reaction at 92.7 kcal/mol. The continuum electrostatic effects of a H_2O environment on top of the inclusion of this one explicit H_2O molecule change the prediction by a only small amount, with the barrier predicted to be 58.5 kcal/mol. We expect the incorporation of nonelectrostatic effects will change this prediction, and this will be investigated when we perform such algorithmic modification in the near future.

Reaction *via* TSB is much more feasible kinetically (E_a 27.0 kcal/mol), with no obvious difference in the thermodynamic energy. Ultimately, this reaction process is the most-reasonable prediction among those proposed, and could well operate *in vivo*.

Conclusions. – In this work, the structure of a series of illudins, **1**–**7**, have been calculated. Special emphasis was placed on **1** and **4**, for which there are X-ray crystallographic data. These same compounds have been studied for their antitumor activity; both are cytotoxic, but **4** is more selective for tumor cells. The reaction path *in vivo* appears to involve initial attack by a thiol-based nucleophile followed by a ring-opening aromatization cascade. From a simple structural comparison, the fulvene series is less reactive and more selective.

Calculations on key reactive species for **1** and **4** correlate to two steps in the reaction, thiol addition to the α,β-unsaturated ketone and the cyclopropylcarbinol ring opening. Thiol attack appears to be rate-determining and is directed by substitute-dents present at C(11). Specifically, the facial selectivity of thiol attack on **1** is controlled thus. This may also provide a way to modify toxicity and selectivity, because thiol attack appears to be a requirement for the reactivity of illudins as antitumor agents. It is known that such a thiol attack is nominally a reversible reaction, enabling the thiol to come on and off in a facile manner; however, the driving force of the cyclopropylcarbinyl ring opening in the second step makes this reversibility no longer feasible. The ring opening occurs with a formal rearrangement of the OH at C(2) to the resulting ethylene chain. Computations favor an intramolecular path in which the OH migration in assisted by a specific bridging H_2O of solvation. New derivatives are being designed to test the model developed from these structure and reactivity studies.

The work was supported by the *National Institutes of Health* (NBCR-RR08605), *National Science Foundation* (CHE-0213323), *Swiss National Fund*, and the GAAN program. Additional support for computational time was provided by the SDSC-ROCKS cluster team.

REFERENCES

[1] T. C. McMorris, M. Anchel, *J. Am. Chem. Soc.* **1965**, *87*, 1594.
[2] T. C. McMorris, A. Kashinatham, R. Lina, H. Rundgren, P. K. Gantzel, M. J. Kelner, R. Sawe, *Phytochem.* **2002**, *61*, 395.
[3] T. C. McMorris, R. Lira, P. K. Gantzel, M. J. Kelner, R. Dawe, *J. Nat. Prod.* **2000**, *63*, 3577.
[4] T. C. McMorris, J. Yu, R. Lira, R. Dawe, J. R. MacDonald, S. J. Waters, A. L. Estes, M. J. Kelner, *J. Org. Chem.* **2001**, *66*, 6158.
[5] T. C. McMorris, M. J. Kelner, W. Wang, L. A. Estes, M. A. Montoya, R. Taetle, *J. Org. Chem.* **1992**, *57*, 6876.

[6] T. C. McMorris, M. J. Kelner, R. K. Chadha, J. S. Siegel, S. S. Moon, M. M. Moya, *Tetrahedron* **1989**, *45*, 5433.
[7] T. C. McMorris, M. J. Kelner, W. Wang, J. Yu, A. Estes, R. Taetle, *J. Nat. Prod.* **1996**, *59*, 896.
[8] T. C. McMorris, *Bioorg. Med. Chem.* **1999**, *7*, 881.
[9] M. J. Kelner, T. C. McMorris, R. Taetle, *J. Natl. Cancer Inst.* **1990**, *82*, 1562.
[10] M. J. Kelner, T. C. McMorris, A. Estes, K. M. Samson, R. D. Bagnell, R. Taetle, *Europ. J. Cancer* **1998**, *34*, 908.
[11] M. J. Kelner, T. C. McMorris, L. Estes, K. M. Samson, N. A. Trani, J. R. MacDonald, *Leukemia* **2000**, *14*, 136.
[12] M. J. Kelner, T. C. McMorris, R. J. Rojas, N. A. Trani, L. A. Estes, *Cancer Chemother. Pharmacol.* **2002**, *49*, 412.
[13] M. J. Kelner, T. C. McMorris, R. J. Rojas, N. A. Trani, T. R. Velasco, L. A. Estes, P. Suthipinijtham, *Invest. New Drugs* **2002**, *20*, 271.
[14] T. C. McMorris, J. Yu, A. Estes, M. J. Kelner, *Tetrahedron* **1997**, *53*, 14579.
[15] T. C. McMorris, M. J. Kelner, W. Wang, S. Moon, R. Taetle, *Chem. Res. Toxicol.* **1990**, *3*, 574.
[16] T. C. McMorris, A. N. Elayadi, J. Yu, Y. Hu, M. J. Kelner, *Drug Metab. Dispos.* **1999**, *27*, 983.
[17] T. C. McMorris, S. S. Moon, M. J. Kelner, *J. Nat. Prod.* **2003**, *66*, 310.
[18] M. W. Schmidt, K. K. Baldridge, J. A. Boatz, J. H. Jensen, S. Koseki, M. S. Gordon, K. A. Nguyen, T. L. Windus, S. T. Albert, *QPEC Bull.* **1990**, *10*, 52.
[19] M. W. Schmidt, K. K. Baldridge, J. A. Boatz, S. T. Elbert, M. S. Gordon, J. H. Jensen, S. Koseki, N. Matsunaga, K. A. Nguyen, S. Su, T. L. Windus, S. T. Elbert, *J. Comp. Chem.* **1993**, *14*, 1347.
[20] M. J. Frisch, G. W. Trucks, H. B. Schlegel, G. E. Scuseria, M. A. Robb, J. R. Cheeseman, V. G. Zakrzewski, J. A. Montgomergy, R. E. Stratmann, J. C. Burant, S. Dapprich, J. M. Millam, A. D. Daniels, K. N. Kudin, M. C. Strain, O. Farkas, J. Tomasi, V. Barone, M. Cossi, R. Cammi, B. Mennucci, C. Pomelli, C. Adamo, S. Clifford, J. Ochterski, G. A. Petersson, P. Y. Ayala, Q. Cui, K. Morokuma, D. K. Malick, A. D. Rabuck, K. Raghavachari, J. B. Foresman, J. Cioslowski, J. V. Ortiz, B. B. Stefanov, G. Liu, A. Liashenko, P. Piskorz, I. Komaromi, R. Gomperts, R. L. Martin, D. J. Fox, T. Keith, M. A. Al-Laham, C. Y. Peng, M. W. Nanayakkara, C. Gonzalez, M. Challocombe, P. M. W. Gill, B. G. Johnson, W. Chen, M. W. Wong, J. L. Andres, M. Head-Gordon, E. S. Replogle, J. A. Pople, Gaussian 98, Revision A.1, *Gaussian, Inc.*, Pittsburgh, PA, 1998.
[21] C. C. J. Roothaan, *Rev. Mod. Phys.* **1951**, *23*, 69.
[22] M. Head-Gordon, J. A. Pople, M. J. Frisch, *Chem. Phys. Lett.* **1988**, *153*, 503.
[23] C. Møller, M. S. Plesset, *Phys. Rev.* **1934**, *46*, 618.
[24] R. G. Parr, W. Yang, 'Density Functional Theory of Atoms and Molecules', Oxford University Press, New York, 1989.
[25] R. G. Parr, *Int. J. Quantum Chem.* **1990**, *37*, 327.
[26] A. D. Becke, *Int. J. Quantum Chem.* **1983**, *23*, 1915.
[27] W. Kohn, L. J. Sham, *Phys. Rev.* **1965**, *140*, A1133.
[28] A. D. Becke, *J. Chem. Phys.* **1993**, *98*, 5648.
[29] C. Lee, W. Yang, R. G. Parr, *Phys. Rev. B: Condens. Matter* **1988**, *37*, 785.
[30] B. Miehlich, A. Savin, H. Stoll, H. Preuss, *Chem. Phys. Lett.* **1989**, *157*, 200.
[31] K. Burke, J. P. Perdew, Y. Wang, 'Electronic Density Functional Theory: Recent Progress and New Directions', Plenum, 1998.
[32] J. P. Perdew, 'Electronic Structure of Solids', Akademie Verlag, Berlin, 1991.
[33] J. P. Perdew, J. A. Chevary, S. H. Vosko, K. A. Jackson, M. R. Pederson, D. J. Singh, C. Fiolhais, *Phys. Rev. B: Condens. Matter* **1992**, *46*, 6671.
[34] J. P. Perdew, J. A. Chevary, S. H. Vosko, K. A. Jackson, M. R. Pedersen, D. J. Singh, *Phys. Rev. B: Condens. Matter* **1993**, *48*, 4978.
[35] C. Adamo, V. Barone, *J. Chem. Phys.* **1998**, *108*, 664.
[36] R. Ditchfield, W. J. Hehre, J. A. Pople, *J. Chem. Phys.* **1971**, *54*, 724.
[37] R. C. Binning Jr., L. A. Curtiss, *J. Comp. Chem.* **1990**, *11*, 1206.
[38] W. J. Hehre, W. A. Lathan, *J. Chem. Phys.* **1972**, *56*, 5255.
[39] M. M. Francl, W. J. Pietro, W. J. Hehre, J. S. Binkley, M. S. Gordon, D. J. DeFrees, J. A. Pople, *J. Chem. Phys.* **1982**, *77*, 3654.
[40] T. H. Dunning Jr., P. J. Hay, 'Modern Theoretical Chemistry', Plenum Press, New York, 1976.
[41] T. H. Dunning Jr., P. J. Hay, 'Methods of Electronic Structure Theory', Plenum Press, New York, 1977.

[42] K. K. Baldridge, J. P. Greenberg, *J. Mol. Graphics* **1995**, *13*, 63.
[43] B. M. Bode, M. S. Gordon, *Mol. Graph. Mod.* **1999**, *16*, 133.
[44] K. Ishida, K. Morokuma, A. Komornicki, *J. Chem. Phys.* **1977**, *66*, 2153.
[45] K. Mueller, *Angew. Chem., Int. Ed.* **1980**, *19*, 1.
[46] C. Gonzalez, H. B. Schlegel, *J. Chem. Phys.* **1989**, *90*, 2154.
[47] C. Gonzalez, H. B. Schlegel, *J. Phys. Chem.* **1990**, *94*, 5523.
[48] E. Gianinetti, M. Raimondi, E. Tornaghi, *Int. J. Quantum Chem.* **1996**, *60*, 157.
[49] K. K. Baldridge, A. Klamt, *J. Chem. Phys.* **1997**, *106*, 6622.
[50] K. K. Baldridge, V. Jonas, *J. Chem. Phys.* **2000**, *113*, 7511.
[51] L. N. Gregerson, K. K. Baldridge, *Helv. Chim. Acta* **2003**, *86*, 4112.
[52] A. Bondi, *J. Phys. Chem.* **1964**, *68*, 441.
[53] A. Klamt, V. Jonas, T. Bürger, C. W. Lohrenz, *J. Phys. Chem.* **1997**, *102*, 5074.
[54] F. Allen, O. Kennard, D. G. Watson, L. Brammer, A. G. Orpen, R. Taylor, *J. Chem. Soc., Perkin Trans. 2* **1987**, S1.
[55] J. A. Pople, R. Krishnan, H. B. Schlegel, J. S. Binkley, *Int. J. Quantum Chem.* **1978**, *14*, 545.
[56] W. J. Hehre, L. Radom, P. v. R. Schleyer, J. A. Pople, 'Ab Initio Molecular Orbital Theory', John Wiley & Sons, New York, 1986.
[57] J. E. Del Bene, *J. Comp. Chem.* **1989**, 603.
[58] G. S. Hammond, *J. Am. Chem. Soc.* **1955**, *77*, 334.
[59] K. Tanaka, T. Inoue, Y. Tezuka, T. Kikuchi, *Chem. Pharm. Bull.* **1996**, *44*, 273.
[60] F. R. Kinder Jr., R.-M. Wang, W. E. Bauta, K. W. Bair, *Bioorg. Med. Chem. Lett.* **1996**, *6*, 1029.
[61] D. Eisenberg, W. Kauzmann, 'The Structure and Properties of Water', Oxford University Press, New York, 1969.
[62] T. H. Lowry, K. H. Richardson, 'Mechanism and Theory in Organic Chemistry', 3rd edn., Harper & Row, New York, 1987.
[63] F. J. P. Leeper, Padma., *Tetrahedron Lett.* **1989**, *30*, 5017.

Received August 31, 2003